JBC Papers in Press. Published on May 30, 2017 as Manuscript M117.792762
The latest version is at http://www.jbc.org/cgi/doi/10.1074/jbc.M117.792762

Molecular dynamics simulations reveal the conformational dynamics of *Arabidopsis thaliana* BRI1 and BAK1 receptor-like kinases

Alexander S. Moffett[1], Kyle W. Bender[2], Steven C. Huber[2,4], and Diwakar Shukla[1,2,3]

From the [1]Center for Biophysics and Quantitative Biology, Department of [2]Plant Biology and [3]Chemical and Biomolecular Engineering, University of Illinois, Urbana, IL 61801, [4]Global Change and Photosynthesis Research Unit, United States Department of Agriculture - Agricultural Research Service, Urbana, IL, 61801

Running title: *Conformational dynamics of* Arabidopsis *receptor-like kinases*

To whom correspondence should be addressed: Diwakar Shukla, diwakar@illinois.edu

Keywords: Conformational change, BAK1, BRI1, protein kinase, plant molecular biology, signal transduction, molecular dynamics, Markov state models

ABSTRACT

The structural motifs responsible for activation and regulation of eukaryotic protein kinases in animals have been studied extensively in recent years, and a coherent picture of their activation mechanisms has begun to emerge. On the other hand, non-animal eukaryotic protein kinases are not as well understood from a structural perspective, representing a large knowledge gap. To this end, we investigated the conformational dynamics of two key *Arabidopsis thaliana* receptor-like kinases, brassinosteroid insensitive 1 (BRI1) and BRI1-associated kinase 1 (BAK1), through extensive molecular dynamics (MD) simulations of their fully phosphorylated kinase domains. MD simulations calculate the motion of each atom in a protein based on classical approximations of interatomic forces, giving researchers insight into protein function at unparalleled spatial and temporal resolutions. We found that in an otherwise "active" BAK1, the αC helix is highly disordered, a hallmark of deactivation, while the BRI1 αC helix is moderately disordered and displays swinging behavior similar to numerous animal kinases. An analysis of all known sequences in the *A. thaliana* kinome found that αC helix disorder may be a common feature of plant kinases.

Eukaryotic protein kinases (ePKs)[1] act as dynamic switches, the units of cellular computation, optimized not for turnover of phosphorylated product, but rather for precise tuning of activation through post-translational modification and protein-protein interaction (1–4). This ability of kinases to respond to multiple inputs allows for adaptable programmed responses integrating numerous signals (4–7). Because of their central role in processing external signals, specifically in relation to cell growth and proliferation and therefore cancer, animal ePKs have long been the target of efforts to understand the structural basis of their activation and regulation, thoroughly reviewed in Refs. 1 & 8.

Several features have been suggested to be necessary for ePK activity (Figure 1), including proximal positioning and proper folding of the αC helix, formation of a salt bridge between the conserved glutamate on the αC helix and the conserved lysine on the β4 sheet (K-E salt bridge), formation of the regulatory and catalytic hydrophobic spines, outward positioning of the conserved phenylalanine

[1]The abbreviations used are: ePK, Eukaryotic protein kinase; BRI1, brassinosteroid insensitive 1; BAK1, BRI1-associated kinase 1; LRR-RLK, leucine-rich repeat receptor-like kinase; RLK, receptor-like kinase; BR, brassinosteroid; MD, molecular dynamics; CD, circular dichroism; MSM, Markov state model; AMD, accelerated MD; ATP, adenosine triphosphate; IDR, intrinsically disordered region; EGFR, epidermal growth factor receptor; RMSD, root mean-squared distance; MSA, multiple sequence alignment

in the DFG motif away from the active site, and unfolding of the activation loop (1, 8)[2]. Careful positioning of these regulatory components is necessary for an ePK to perform catalysis, meaning that any conformation with a regulatory structure out of place is inactive. Despite the resultantly enormous multiplicity of possible inactive states, several distinct conformations recur throughout the ePKs. For example, the human cytoplasmic tyrosine kinase Src takes on an inactive conformation where the unphosphorylated activation loop folds and obscures the active site and the αC helix swings away from the active site in concert with breakage of the K-E salt bridge (9, 10) (references to a "Src-like" state throughout this paper will exclusively denote distal swinging of the αC helix).

Because of the focus of research on ePKs has been in clades directly relevant to medicine (i.e. the vertebrates), it remains unclear how similar the activation processes of non-animal ePKs are to those in animals. Given the highly conserved nature of ePK structures across the eukaryotes (1), some insight into non-animal eukaryote ePK activation can be gleaned from the expansive structural information available from animal systems; however, the possibility of unique activation mechanisms not found in animal ePKs remains.

Brassinosteroid-insensitive 1 (BRI1) and BRI1-associated kinase 1 (BAK1) are members of the leucine-rich repeat receptor-like kinases (LRR-RLKs), a group of structurally similar membrane receptors within the monophyletic receptor-like kinase (RLK) clade, which is homologous to and shares functional characteristics with the animal Pelle kinases (11). While LRR-RLKs are intrinsic membrane proteins, each with an extracellular domain, a single transmembrane helix, a juxtamembrane domain, and an intracellular dual-specificity kinase domain, we have performed simulations of each kinase domain in isolation. These two proteins play a critical role in control of plant growth and development along with other processes (12–14), associating and reciprocally phosphorylating one another upon binding of a brassinosteroid (BR) hormone to the BRI1 extracellular domain (15–19). Activation of BRI1 and BAK1 triggers a downstream cascade of phosphorylation and dephosphorylation events causing alteration of gene expression and ultimately plant growth (13, 20, 21).

Here, we studied the conformational dynamics of the *Arabidopsis thaliana* BRI1 and BAK1 through atomistic molecular dynamics (MD) simulation. Biomolecular MD simulation uses the initial coordinates of all atoms from a crystal structure as an input, assigns an initial velocity to each atom, and numerically integrates the classical equations of motion to yield a trajectory through time. Interactions between atoms are represented in approximate form, with parameters chosen according to experiments and quantum mechanical calculations. Although structural biology techniques are constantly improving in their ability to resolve protein structures, MD simulation provides unparalleled detail into the conformational dynamics of biomolecules (22, 23). With the power of this technique, we sought to characterize the conformational dynamics governing the activity of BRI1 and BAK1, specifically in terms of known ePK activation features.

RESULTS

In order to identify the structural features important for BRI1 and BAK1 activation, we performed extensive molecular dynamics simulations of their isolated kinase domains. Despite the fact that the simulated BRI1 kinase domain was fully phosphorylated, a necessary condition for complete BRI1 activation, we observed a high degree of αC helix disorder and breaking of the conserved K-E salt bridge (Figure 2**a**). Still, the active-like state is the most stable region (Figure 2**a**, region I) although there does not appear to be a free energy barrier to unfolding of the αC helix with the K-E salt bridge formed (Figure 2**a**, region II) until there is already a significant degree of disorder. It is unclear how this unfolding behavior concurrent with a formed K-E salt bridge affects catalytic activity. Disorder in the BRI1 αC helix is supported by CD spectroscopy experiments of the isolated BRI1 αC helix peptide, showing an intermediate degree of helicity as compared to the disordered human epidermal growth

[2]In BRI1 and BAK1, these features correspond to: conserved glutamate (BRI1: E927, BAK1: E334), conserved lysine (BRI1: K911, BAK1: K317), and conserved DFG phenylalanine (BRI1: F1028, BAK1: F435).

factor receptor (EGFR) and helical hSrc αC helix peptides (Figure S1).

The K-E salt bridge can be broken while the αC helix remains ordered (Figure 2**a**, unlabeled region above region I) likely due to interaction between K911 and ATP, while further distance between K911 and E927 coincides with greater fluctuation in the same distance. The region characterized by a large distance between K911 and E927 (Figure 2**a**, regions III and IV) covers a similar range of αC helix disorder to the region with a formed K-E salt bridge (Figure 2**a**, regions I and II).

The distance between K911 and E927 is measured between the terminal nitrogen atom in lysine and the δ-carbon in glutamate, meaning that changes in this distance while the αC helix remains ordered could be caused by conformational changes in the side chains, swinging of the αC helix outward, or some combination of the two. Region III in Figure 2**a**, represents breaking of the K-E salt bridge coupled with distal movement of the αC helix (Figure S2). This suggests the presence of a Src-like inactive state in BRI1, where the αC helix remains folded but swings outward from its active-like position, breaking the K-E salt bridge while preventing rapid reformation by conformational changes in the side chains alone. The Src-like inactive state represents the second most stable region of the free energy landscape, possibly meaning that transitions to this state are the main mechanism of BRI1 deactivation when only considering its internal conformational dynamics. E927 interacts extensively with R1032 on the activation loop when the E927-K911 interaction is broken (Figure S3) in a similar manner to human Src kinase (24).

Similarly to BRI1, BAK1 has an active-like state (Figure 3**a**, region I), a region with αC helix disorder but retaining the K-E salt bridge (Figure 3**a**, region II), and a state with a folded and active-like positioned αC helix and a broken K-E salt bridge due to interaction between K317 and ATP (Figure 3**a**, region III). However, BAK1 does not take on a Src-like inactive conformation, as there is no distal swinging of the folded αC helix (Figure S4), and minimal interaction between E334 and K439, the lysine residue in the analogous position on the activation loop to BRI1 R1032 (Figure S5). Furthermore, conformations with a marginally broken K-E salt bridge are far less stable in BAK1 as compared with BRI1 (Figure 3**a** & **b**, region III). The most striking feature of the BAK1 free energy landscape is the large, well-populated area where the αC helix is highly disordered (Figure 3**a**, region IV), allowing for a large range of distances between K317 and E334. Breaking of the K-E salt bridge allows for a greater extent of αC helix disorder in BAK1 than in BRI1.

It is unclear whether the disorder in the BAK1 and BRI1 αC helices are primarily due to interaction with neighboring residues or intrinsic disorder of the αC helix itself. In the former case, a stable αC helix sequence of another kinase substituted for the native sequence would likely also display disorder. Due to issues with solubility for the BAK1 αC helix peptide, instead of performing CD spectroscopy we substituted the otherwise stable hSrc αC helix for the native BAK1 αC helix sequence *in silico*. We find that the hSrc αC helix remains stable relative to the native BAK1 helix, eliminating a large portion of the unfolded region (Figure 4**a**, region IV) though still allowing for notable deviation from a purely helical form (Figure 4**a**, regions II and IV). All together, this suggests the presence of intrinsic disorder, although we can not rule out a role for structural context from these results alone.

In addition to the stabilized αC helix, the conserved K-E salt bridge is also stabilized, where the αC helix remains folded in the main region of breakage (Figure 4**a**, region III). As with native BAK1 there does not appear to be a Src-like inactive state (Figure S6).

Although the extent of unfolding of the Src αC helix is less than the native BAK1 αC helix, there is little barrier to partial unfolding when the K-E salt bridge is formed. Regions I and II of Figure 4**a** appear to constitute a kinetically indistinct state where the BAK1-Src αC helix can partially unfold and refold while constrained by the K-E salt bridge, while breaking of the K-E salt bridge occurs primarily by way of region I into region III over a free energy barrier of approximately 2-3 kcal·mol^{-1}. This transition is likely due to a rotation of the lysine side chain towards the negatively charged ATP phosphate groups as is seen in native BRI1 and BAK1. Interestingly, there is a small, low free energy re-

gion near 0.4 αC helix helical content and 20 Å K-E salt bridge distance (Figure 4**a**, above region IV). However, the low free energy of this region is likely due to sampling error (see Supplementary Data for further discussion).

In order to investigate the universality of αC helix disorder in the *A. thaliana* kinome, we obtained a previously identified set of 930 *A. thaliana* ePK sequences (25) and used the PONDR-Fit web server (26) to predict disorder propensities of residues in putative αC helix regions and mapped the predicted disorder propensities onto a previously published *A. thaliana* kinome phylogenetic tree (Figure 5**a**) (25). It is evident from this tree that αC helix disorder is predicted to be widespread across the *A. thaliana* kinome, suggesting that transitions between ordered and disordered states in this region could be a common regulatory mechanism. We repeated the same analysis for the *Oryza sativa* (Figures S7 & S8) and human kinomes (Figures S9 & S10), finding similar levels of disorder in putative αC helix regions.

As a check for consistency with our simulations, we find that the hSrc sequence is predicted to have low disorder across the αC helix region, while hEGFR and BRI1 are predicted to display disorder qualitatively similar to the average *A. thaliana* ePK (Figure 5**b**). BAK1 on the other hand displays disorder near the upper boundary of the interquartile range for all examined residues (Figure 5**b**), and is clearly on the upper tail of the distribution of average αC helix residue disorder (Figure 5**c**). Several ePK families are predicted to have a majority of members with high αC helix disorder, including the CRR, NEK, and SnRK1 families (Figure S11).

DISCUSSION

It is no surprise that BRI1 and BAK1 would be heavily regulated given their great importance in plant growth and development (14, 27–31). Intrinsic disorder in BAK1 and, to a lesser extent, BRI1 αC helices may be one such mechanism of regulation. Given that fully phosphorylated, ATP-bound BRI1 and BAK1 were able to spontaneously transition from active-like to inactive conformations characterized by broken K-E salt bridges and varying degrees of αC helix unfolding, the presence of intrinsic αC disorder could provide insight into how BRI1-BAK1 association leads to their activation. It is possible that αC helix stabilization due to physical interaction between BRI1 and BAK1 is necessary for activation in addition to phosphorylation in a similar fashion to the metazoan EGFR, a receptor tyrosine kinase implicated in multiple cancers (9, 32, 33).

In human EGFR, disorder in the αC helix is believed to be suppressed by ligand-induced homodimerization and formation of an asymmetric dimer in the kinase domains, with one kinase acting as an activator for the other (9, 33, 34). By comparison with hEGFR, our discovery of highly populated states in large timescale MD simulations of the BRI1 and BAK1 kinase domains characterized by disorder in the αC helices suggests that dimerization of BRI1 and BAK1 might promote catalytically competent conformations of both proteins via stabilization of their respective αC helices, as has been suggested previously based on the similarity of inhibitor binding interfaces in hEGFR and BRI1 (32). However, as we have simulated BRI1 and BAK1 isolated from all potentially interacting proteins and relieved of their juxtamembrane and C-terminal tail domains, there are other mechanisms through which BRI1 and BAK1 could suppress αC helix disorder and pointed experiments are needed to provide more definitive evidence for this hypothesis.

To the best of our knowledge, EGFR is the only other ePK that displays αC helix disorder in previous MD studies (33). This could be more due to the small fraction of ePKs which have been simulated than general stability of the αC helix, given the high levels of disorder we have predicted in three different kinomes. However, there is αC helix disorder in a crystal structure of human AKT1, caused by inhibitor binding (35).

Additionally, distal swinging of the αC helix away from the active site is a well established mechanism of deactivation in numerous animal ePKs, where interactions with regulatory domains or other kinases causes proximal relocation of the αC helix and subsequent activation (1, 9, 34, 36). BRI1 is able to transition to a similar Src-like inactive state in our simulations, suggesting that BRI1 may fit within the paradigms of animal ePK allosteric control. Distal swinging of the αC helix is commonly observed in MD simulations of mammalian protein kinases, including human Lyn and CDK2 (37), EGFR (38), and Src (10), and through analysis of available crys-

tal structures (36, 37). In contrast, BAK1 does not have a well-defined inactive state which complicates inference of an activation pathway without considering interactions with BRI1 or other LRR-RLKs.

It is also worth noting that the conditions of our simulations preclude a flip of the DFG motif phenylalanine into the ATP binding pocket, as ATP is already bound, and we see no Src-like folding of the activation loop into a helix (Figure S12) presumably due to the phosphorylation state of the simulated proteins. However, these regulatory mechanisms may also play a role in BRI1 and BAK1 activation and future simulations of the unphosphorylated, apo kinase domains could address this question.

Intrinsically disordered regions (IDRs) are thought to confer versatility to proteins in terms of their interaction partners, and there is evidence that IDRs are enriched in protein-protein interaction network hub proteins (39, 40), including hubs in kinase interaction networks (41). BAK1, which has considerable αC helix disorder in our simulations, is known to have an important role not just in brassinosteroid signaling, but also in innate immunity, cell death control, and light response, associating with several other LRR-RLKs (42, 43). It is possible that BAK1 is able to form active dimers with multiple LRR-RLKs because of intrinsic disorder in its αC helix. While it is not known how BAK1 interacts with other LRR-RLKs, disorder in the BAK1 αC helix and similarities between a protein binding site inhibiting dimerization of hEGFR and the corresponding region of BRI1 (32) could point to EGFR-like complex formation. In that case, the αC helix of BAK1 could serve as a general interaction surface with BRI1 and other LRR-RLKs.

Given that αC helix disorder is expected throughout a large fraction of the *A. thaliana* kinome (Figure 5), it seems possible that this regulatory mechanism is present in multiple other plant ePKs. Both the *O. sativa* (Figures S7 & S8) and human kinomes (Figures S9 & S10) display similar profiles of αC helix disorder to the *A. thaliana* kinome. For the human kinome, this result is consistent with a previous analysis finding that 83% of human ePKs contain at least one IDR somewhere in their kinase domain (41). High levels of αC helix disorder in the kinomes of two evolutionarily distant groups of organisms could indicate that stabilization of the αC helix is a general strategy for ePK activation across the eukaryotes. However, more evidence is needed to substantiate the universality of αC helix disorder in ePKs.

The activation pathways of BRI1 and BAK1 are still unknown as there are no inactive, unphosphorylated structures available for either receptor (Figure S13). Future studies will need to address how phosphorylation contributes to BRI1 and BAK1 activation as a necessary but apparently insufficient step.

EXPERIMENTAL PROCEDURES

Simulation details — All simulations were performed using the AMBER 14 molecular dynamics package (44) and the CHARMM36 force field (45–47) on the Blue Waters petascale computing facility. All simulation systems were set up using the VMD (48) plugin Psfgen 1.6 and converted to Amber format using the CHAMBER software tool (49). Starting coordinates for BRI1 and BAK1 kinase domains were taken from available crystal structures (BRI1 PDB ID: 4OA2 (50); BAK1 PDB IDs: 3TL8 (chains A, D, G, and H) (51), 3UIM (29), and 3ULZ (52)) (see Figure S14 for exact sequences and Table S3 for phosphorylation states). All segments missing from the BRI1 and BAK1 crystal structures were modeled using the SwissModel webserver (53). In order to create the chimeric BAK1 kinase the αC helix of hSrc kinase (PDB ID: 1Y57 (54)) was grafted into the 3ULZ and 3UIM structures in place of the native αC helix (see Figure S14 for exact sequence).

Starting structures were solvated in water boxes with dimensions of approximately 90 Å X 70 Å X 63 Å with TIP3P model molecules (55). Sodium and chloride ions were added to neutralize the charge of all systems and bring salt concentration to approximately 150 mM. An ATP molecule with two magnesium ions bound, taken from previous simulations, was inserted into the binding pocket for all structures in place of the modified adenosine-phosphate molecules used in crystallization, aligned with the adenosine ring of the corresponding ATP analogue. All systems were subjected to 10,000 steps of energy minimization and were equilibrated for 8-10 ns in an NPT ensemble at 300K and 1 atm, maintained using Langevin dynamics and a Berendsen barostat. Simulations were performed using a

2 fs time step, periodic boundary conditions, particle mesh Ewald electrostatics (56), and constraints of hydrogen-containing bonds using the SHAKE algorithm (57, 58). Equilibrated structures were then equilibrated for another 10 ns to obtain average dihedral angle potential energies for calculation of accelerated MD (AMD) (59) parameters (Table S4) according to reference (60).

For BAK1, ten replicates of each of the six structures were simulated using AMD for a total time given in Table S5. BRI1 AMD simulations were initiated from a single crystal structure, and two rounds of adaptive AMD sampling were performed, first with a single trajectory and for the second and third rounds with 25 trajectories run in parallel for a total simulation time given in Table S5. Finally, 25 AMD simulations were run in parallel serially for a total time indicated in Table S5. Similarly, BAK1-Src AMD simulations were initiated from each of the two structures indicated in Table S4 and run for one round of adaptive AMD with 25 parallel trajectories, and finally run with 25 trajectories in parallel serially for total times indicated in Table S5. Ideally the AMD simulation strategy for all three systems would be identical, and it is possible that some of the differences observed between the free energy landscapes of each system could be due in part to differences in sampling schemes. The final round of AMD sampling for each system was clustered in the space of the distance between the most distal side chain nitrogen in the lysine and carbon in glutamate within the conserved K-E salt bridge and αC helix RMSD from the crystal structures (or initial structure, for the BAK1-Src chimera) into 100 states, and the nearest neighbors of the cluster centroids were chosen as starting structures for unbiased simulation. An aggregate of 30-40 μs of unbiased MD simulation time was performed for each system (Table S5).

Markov state model construction — The entire Markov state model (MSM) construction process was performed using the MSMBuilder 3 Python package for all systems (61). All trajectories were subsampled so that the time difference between consecutive frames in a trajectory was 200 ps. We chose the RMSD of the atoms contained in the αC helix and separately the N-terminal lobe excluding the αC helix with respect to the corresponding reference structure (BRI1, PDB: 4OA2 (50); BAK1, PDB: 3TL8, chain A (51); initial structure of BAK1-Src, PDB: 1Y57 (54) for the αC helix, PDB: 3UIM (29) and 3ULZ (52) for the remainder of the kinase) as features for construction of MSMs for our systems of interest. Each of the two metrics for BRI1 and BAK1 trajectories were normalized by subtracting the mean and dividing by the standard deviation, where both statistics were calculated over all trajectories from the appropriate protein. The ranges of valid lag times for the BRI1, BAK1, and BAK1-Src models were both chosen to be 50-150 ns based on convergence of implied timescales across models built with a range of cluster numbers (Figures S15, S16, & S17). We then used the Osprey variational cross-validation package to select lag times of 50 ns for all three models and cluster numbers of 278, 319, and 386 for the BRI1, BAK1, and BAK1-Src models, respectively, which maximized the model generalized matrix Rayleigh quotient cross-validation scores using shuffle-split cross-validation (62). Using these MSM parameters, we estimated reversible maximum likelihood transition probability matrices for all models.

Error analysis was conducted by constructing Bayesian MSMs (63) with the same parameters as the corresponding maximum likelihood MSMs, utilizing Metropolis Markov chain Monte Carlo to sample the prior distribution of transition matrices.

Free energy plots were constructed by first creating normalized a two-dimension histogram for each of N states, using the structures in each state projected onto the distance between the glutamate δ-carbon atom and the lysine side-chain nitrogen in the conserved K-E salt bridge and the helical content of the αC helix, as defined in the NAMD 2.11 manual (64) as detailed above. Each state histogram [$h_i(x, y)$ for state i] for the given model was then weighed by the equilibrium probability (π_i) of the corresponding state calculated from the transition probability matrix and summed together, according to the following equation:

$$F(x, y) = -RT \log \left[\sum_{i=1}^{N} \pi_i h_i(x, y) \right] \qquad (1)$$

where R is the gas constant and T is the temperature.

Bioinformatic analysis — The list of the 940 *A. thaliana* kinases identified by Zulawski et al. (25)

was used to create a multiple sequence alignment (MSA) using Clustal Omega (65) after the kinase sequences were retrieved from the Arabidopsis Information Resource (66). Using the Biopython package, (67) the position of the conserved glutamate in the αC helix (BAK1: 334, BRI1: 927) in the MSA was identified, and every kinase without a gap at that position was selected for further analysis (a total of 930 out of the original 940 sequences). Sequences putatively containing the αC helix of each kinase were produced by taking a subsequence consisting of the conserved glutamate position and 20 residues in both directions for a total of 41 residues. All 930 subsequences were submitted to the PONDR-Fit consensus disorder prediction web server (26), and the average disorder propensity over the 15 residue segment corresponding to the BAK1 αC helix for each sequence was calculated and mapped onto the *A. thaliana* kinome phylogenetic tree from Zulawski et al. (25) using FigTree 1.4.2 (68).

Acknowledgments: The authors thank the Blue Waters sustained-petascale computing project, which is supported by the National Science Foundation (awards OCI-0725070 and ACI-1238993) and the state of Illinois, for providing computing time for this study.

Conflict of interest: The authors declare that they have no conflicts of interest with the contents of this article.

Author contributions: SCH and DS conceived the study. ASM performed and analyzed simulations. KWB performed and analyzed experiments. ASM, KWB, and DS created figures. ASM and KWB wrote the manuscript. ASM, KWB, SCH, and DS edited the manuscript.

REFERENCES

1. Taylor, S. S. and Kornev, A. P. (2011) Protein kinases: Evolution of dynamic regulatory proteins, *Trends Biochem. Sci.* **36**(2), 65–77. 10.1016/j.tibs.2010.09.006
2. Hunter, T. (1987) A thousand and one protein kinases, *Cell* **50**(6), 823–829. 10.1016/0092-8674(87)90509-5
3. Hardie, D. (1999) Plant protein serine/threonine kinases: Classification and functions, *Ann. Rev. Plant Biol.* **50**, 97–131. 10.1146/annurev.arplant.50.1.97
4. Bray, D. (1995) Protein molecules as computational elements in living cells, *Nat.* **376**(6538), 307–312. 10.1038/376307a0
5. Cohen, P. (1992) Signal integration at the level of protein kinases, protein phosphatases and their substrates, *Trends Biochem. Sci.* **17**(10), 408–413. 10.1016/0968-0004(92)90010-7
6. Tyson, J. J., Chen, K. C., and Novak, B. (2003) Sniffers, buzzers, toggles and blinkers: Dynamics of regulatory and signaling pathways in the cell, *Curr. Opin. Cell Biol.* **15**(2), 221–231. 10.1016/S0955-0674(03)00017-6
7. Kholodenko, B. N. (2006) Cell-signalling dynamics in time and space, *Nat. Rev. Mol. Cell Biol.* **7**, 165–176. 10.1038/nrm1838
8. Endicott, J. A., Noble, M. E., and Johnson, L. N. (2012) The structural basis for control of eukaryotic protein kinases, *Annu. Rev. Biochem.* **81**, 587–613. 10.1146/annurev-biochem-052410-090317
9. Jura, N., Zhang, X., Endres, N. F., Seeliger, M. A., Schindler, T., and Kuriyan, J. (2011) Catalytic control in the EGF receptor and its connection to general kinase regulatory mechanisms, *Mol. Cell* **42**(1), 9–22. 10.1016/j.molcel.2011.03.004
10. Shukla, D., Meng, Y., Roux, B., and Pande, V. S. (2014) Activation pathway of Src kinase reveals intermediate states as targets for drug design, *Nat. Comm.* **5**. 10.1038/ncomms4397
11. Shiu, S.-H. and Bleecker, A. B. (2001) Receptor-like kinases from form a monophyletic gene family related to animal receptor kinases, *Proc. Natl. Acad. Sci. U.S.A.* **98**(19), 10763–10768. 10.1073/pnas.181141598
12. Zhu, J.-Y., Sae-Seaw, J., and Wang, Z.-Y. (2013) Brassinosteroid signalling, *Dev.* **140**(8), 1615–1620. 10.1242/dev.060590
13. Wang, Z.-Y., Bai, M.-Y., Oh, E., and Zhu, J.-Y. (2012) Brassinosteroid signaling network and regulation of photomorphogenesis, *Annu. Rev. Genet.* **46**, 701–724. 10.1146/annurev-genet-102209-163450
14. Wang, W., Bai, M.-Y., and Wang, Z.-Y. (2014) The brassinosteroid signaling network - a paradigm of signal integration, *Curr. Opin. Plant Biol.* **21**, 147–153. 10.1016/j.pbi.2014.07.012
15. She, J., Han, Z., Kim, T.-W., Wang, J., Cheng, W., Chang, J., Shi, S., Wang, J., Wang, Z.-Y., and Chai, J. (2011) Structural insight into brassinosteroid perception by BRI1, *Nat.* **474**, 472–476. 10.1038/nature10178
16. Caño-Delgado, A., Yin, Y., Yu, C., Vafeados, D., Mora-García, S., Cheng, J.-C., Nam, K. H., Li, J., and Chory, J. (2004) BRL1 and BRL3 are novel brassinosteroid receptors that function in vascular differentiation in *Arabidopsis*, *Dev.* **131**(21), 5341–5351. 10.1242/dev.01403
17. Wang, X., Kota, U., He, K., Blackburn, K., Li, J., Goshe, M. B., Huber, S. C., and Clouse, S. D. (2008) Sequential transphosphorylation of the BRI1/BAK1 receptor kinase complex impacts early events in brassinosteroid signaling, *Dev. Cell* **15**(2), 220–235. 10.1016/j.devcel.2008.06.011
18. Santiago, J., Henzler, C., and Hothorn, M. (2013) Molecular mechanism for plant steroid receptor activation by somatic embryogenesis co-receptor kinases, *Sci.* **341**(6148), 889–892. 10.1126/science.1242468
19. Sun, Y., Han, Z., Tang, J., Hu, Z., Chai, C., Zhou, B., and Chai, J. (2013) Structure reveals that BAK1 as a co-receptor recognizes the BRI1-bound brassinolide, *Cell Res.* **23**(11), 1326. 10.1038/cr.2013.131

20. Sun, Y., Fan, X.-Y., Cao, D.-M., Tang, W., He, K., Zhu, J.-Y., He, J.-X., Bai, M.-Y., Zhu, S., Oh, E., Patil, S., Kim, T.-W., Ji, H., Wong, W. H., Rhee, S. Y., and Wang, Z.-Y. (2010) Integration of brassinosteroid signal transduction with the transcription network for plant growth regulation in *Arabidopsis*, *Dev. Cell* **19**(5), 765–777. 10.1016/j.devcel.2010.10.010
21. Singh, A. P. and Savaldi-Goldstein, S. (2015) Growth control: brassinosteroid activity gets context, *J. Exp. Bot.* **66**(4), 1123–1132. 10.1093/jxb/erv026
22. Lee, E. H., Hsin, J., Sotomayor, M., Comellas, G., and Schulten, K. (2009) Discovery through the computational microscope, *Struct.* **17**(10), 1295–1306. 10.1016/j.str.2009.09.001
23. Dror, R. O., Dirks, R. M., Grossman, J., Xu, H., and Shaw, D. E. (2012) Biomolecular simulation: a computational microscope for molecular biology, *Annu. Rev. Biophys.* **41**, 429–452. 10.1146/annurev-biophys-042910-155245
24. Ozkirimli, E., Yadav, S. S., Miller, W. T., and Post, C. B. (2008) An electrostatic network and long-range regulation of src kinases, *Protein Sci.* **17**(11), 1871–1880. 10.1110/ps.037457.108
25. Zulawski, M., Schulze, G., Braginets, R., Hartmann, S., and Schulze, W. X. (2014) The *Arabidopsis* kinome: Phylogeny and evolutionary insights into functional diversification, *BMC Genom.* **15**(1), 548. 10.1186/1471-2164-15-548
26. Xue, B., Dunbrack, R. L., Williams, R. W., Dunker, A. K., and Uversky, V. N. (2010) PONDR-FIT: A meta-predictor of intrinsically disordered amino acids, *Biochim. Biophys. Acta* **1804**(4), 996–1010. 10.1016/j.bbapap.2010.01.011
27. Wang, X., Li, X., Meisenhelder, J., Hunter, T., Yoshida, S., Asami, T., and Chory, J. (2005) Autoregulation and homodimerization are involved in the activation of the plant steroid receptor BRI1, *Dev. Cell* **8**(6), 855–865. 10.1016/j.devcel.2005.05.001
28. Wang, X. and Chory, J. (2006) Brassinosteroids regulate dissociation of BKI1, a negative regulator of BRI1 signaling, from the plasma membrane, *Sci.* **313**(5790), 1118–1122. 10.1126/science.1127593
29. Yan, L., Ma, Y., Liu, D., Wei, X., Sun, Y., Chen, X., Zhao, H., Zhou, J., Wang, Z., Shui, W., and Lou, Z. (2012) Structural basis for the impact of phosphorylation on the activation of plant receptor-like kinase BAK1, *Cell Res.* **22**(8), 1304. 10.1038/cr.2012.74
30. Jaillais, Y., Hothorn, M., Belkhadir, Y., Dabi, T., Nimchuk, Z. L., Meyerowitz, E. M., and Chory, J. (2011) Tyrosine phosphorylation controls brassinosteroid receptor activation by triggering membrane release of its kinase inhibitor, *Gene. Dev.* **25**(3), 232–237. 10.1101/gad.2001911
31. Oh, M.-H., Clouse, S. D., and Huber, S. C. (2012) Tyrosine phosphorylation of the BRI1 receptor kinase occurs via a post-translational modification and is activated by the juxtamembrane domain, *Front Plant Sci.* **3**, 175. 10.3389/fpls.2012.00175
32. Belkhadir, Y. and Jaillais, Y. (2015) The molecular circuitry of brassinosteroid signaling, *New Phytol.* **206**(2), 522–540. 10.1111/nph.13269
33. Shan, Y., Eastwood, M. P., Zhang, X., Kim, E. T., Arkhipov, A., Dror, R. O., Jumper, J., Kuriyan, J., and Shaw, D. E. (2012) Oncogenic mutations counteract intrinsic disorder in the EGFR kinase and promote receptor dimerization, *Cell* **149**(4), 860–870. 10.1016/j.cell.2012.02.063
34. Endres, N. F., Barros, T., Cantor, A. J., and Kuriyan, J. (2014) Emerging concepts in the regulation of the EGF receptor and other receptor tyrosine kinases, *Trends Biochem. Sci.* **39**(10), 437–446. 10.1016/j.tibs.2014.08.001
35. Wu, W.-I., Voegtli, W. C., Sturgis, H. L., Dizon, F. P., Vigers, G. P., and Brandhuber, B. J. (2010) Crystal structure of human akt1 with an allosteric inhibitor reveals a new mode of kinase inhibition, *PLoS One* **5**(9), e12913. 10.1371/journal.pone.0012913
36. Palmieri, L. and Rastelli, G. (2013) αC helix displacement as a general approach for allosteric modulation of protein kinases, *Drug Discov. Today* **18**(7), 407–414. 10.1016/j.drudis.2012.11.009
37. Huang, H., Zhao, R., Dickson, B. M., Skeel, R. D., and Post, C. B. (2012) αC helix as a switch in the

conformational transition of Src/CDK-like kinase domains, *J. Phys. Chem. B* **116**(15), 4465–4475. 10.1021/jp301628r

38. Shan, Y., Arkhipov, A., Kim, E. T., Pan, A. C., and Shaw, D. E. (2013) Transitions to catalytically inactive conformations in egfr kinase, *Proc. Natl. Acad. Sci. USA* **110**(18), 7270–7275. 10.1073/pnas.1220843110
39. Kim, P. M., Sboner, A., Xia, Y., and Gerstein, M. (2008) The role of disorder in interaction networks: A structural analysis, *Mol. Syst. Biol.* **4**(1), 179. 10.1038/msb.2008.16
40. Malaney, P., Pathak, R. R., Xue, B., Uversky, V. N., and Davé, V. (2013) Intrinsic disorder in PTEN and its interactome confers structural plasticity and functional versatility, *Sci. Rep.* **3**. 10.1038/srep02035
41. Kathiriya, J. J., Pathak, R. R., Clayman, E., Xue, B., Uversky, V. N., and Davé, V. (2014) Presence and utility of intrinsically disordered regions in kinases, *Mol. Biosyst.* **10**(11), 2876–2888. 10.1039/c4mb00224e
42. Chinchilla, D., Shan, L., He, P., de Vries, S., and Kemmerling, B. (2009) One for all: The receptor-associated kinase BAK1, *Trends Plant Sci.* **14**(10), 535–541. 10.1016/j.tplants.2009.08.002
43. Liebrand, T. W., van den Burg, H. A., and Joosten, M. H. (2014) Two for all: Receptor-associated kinases SOBIR1 and BAK1, *Trends Plant Sci.* **19**(2), 123–132. 10.1016/j.tplants.2013.10.003
44. Case, D. A., Berryman, J. T., Betz, R. M., Cerutti, D. S., Cheatham, T. E. I., Darden, T. A., Duke, R. E., Giese, T. J., Gohlke, H., Goetz, A. W., Homeyer, N., Izadi, S., Janowski, P., Kaus, J., Kovalenko, A., Lee, T. S., LeGrand, S., Li, P., Luchko, T., Luo, R., Madej, B., Merz, K. M., Monard, G., Needham, P., Nguyen, H. T., Omelyan, I., Onufriev, A., Roe, D. R., Roitberg, A., Salomon-Ferrer, R., Simmerling, C. L., Smith, W., Swails, J., Walker, R. C., Wang, J., Wolf, R. M., Wu, X., York, D. M., and Kollman, P. A. (2015) AMBER 2015, University of California, San Francisco
45. MacKerell Jr., A. D., Bashford, D., Bellott, M., Dunbrack, R., Evanseck, J., Field, M. J., Fischer, S., Gao, J., Guo, H., Ha, S., Joseph-McCarthy, D., Kuchnir, L., Kuczera, K., Lau, F., Mattos, C., Michnick, S., Ngo, T., Nguyen, D., Prodham, B., Reiher III, W., Roux, B., Schlenkrich, M., Smith, J., Stote, R., Straub, J., Watanabe, M., Wiórkiewicz-Kuczera, J., Yin, D., and Karplus, M. (1998) All-atom empirical potential for molecular modeling and dynamics studies of proteins, *J. Phys. Chem. B* **102**(18), 3586–3616. 10.1021/jp973084f
46. Best, R. B., Zhu, X., Shim, J., Lopes, P. E., Mittal, J., Feig, M., and MacKerell Jr., A. D. (2012) Optimization of the additive CHARMM all-atom protein force field targeting improved sampling of the backbone ϕ, ψ and side-chain χ_1 and χ_2 dihedral angles, *J. Chem. Theory Comput.* **8**(9), 3257–3273. 10.1021/ct300400x
47. Vanommeslaeghe, K., Hatcher, E., Acharya, C., Kundu, S., Zhong, S., Shim, J., Darian, E., Guvench, O., Lopes, P., Vorobyov, I., and MacKerell Jr., A. D. (2010) CHARMM general force field: A force field for drug-like molecules compatible with the CHARMM all-atom additive biological force fields, *J. Comput. Chem.* **31**(4), 671–690. 10.1002/jcc.21367
48. Humphrey, W., Dalke, A., and Schulten, K. (1996) VMD: Visual molecular dynamics, *J. Mol. Graph.* **14**(1), 33–38. 10.1016/0263-7855(96)00018-5
49. Crowley, M. F., Williamson, M. J., and Walker, R. C. (2009) CHAMBER: Comprehensive support for CHARMM force fields within the AMBER software, *Int. J. Quant. Chem.* **109**(15), 3767–3772. 10.1002/qua.22372
50. Bojar, D., Martinez, J., Santiago, J., Rybin, V., Bayliss, R., and Hothorn, M. (2014) Crystal structures of the phosphorylated BRI1 kinase domain and implications for brassinosteroid signal initiation, *Plant J.* **78**(1), 31–43. 10.1111/tpj.12445
51. Cheng, W., Munkvold, K. R., Gao, H., Mathieu, J., Schwizer, S., Wang, S., Yan, Y.-b., Wang, J., Martin, G. B., and Chai, J. (2011) Structural analysis of *Pseudomonas syringae* AvrPtoB bound to

host BAK1 reveals two similar kinase-interacting domains in a type III effector, *Cell Host Microbe* **10**(6), 616–626. 10.1016/j.chom.2011.10.013

52. Lou, Z. Y., Yan, L. M., and Ma, Y. Y. (2012) 3ULZ: Crystal structure of apo BAK1, 10.2210/pdb3ulz/pdb
53. Biasini, M., Bienert, S., Waterhouse, A., Arnold, K., Studer, G., Schmidt, T., Kiefer, F., Cassarino, T. G., Bertoni, M., Bordoli, L., and Schwede, T. (2014) SWISS-MODEL: Modelling protein tertiary and quaternary structure using evolutionary information, *Nucleic Acids Res.* , W252–W258. 10.1093/nar/gku340
54. Cowan-Jacob, S. W., Fendrich, G., Manley, P. W., Jahnke, W., Fabbro, D., Liebetanz, J., and Meyer, T. (2005) The crystal structure of a c-Src complex in an active conformation suggests possible steps in c-Src activation, *Struct.* **13**(6), 861–871. 10.1016/j.str.2005.03.012
55. Jorgensen, W. L., Chandrasekhar, J., Madura, J. D., Impey, R. W., and Klein, M. L. (1983) Comparison of simple potential functions for simulating liquid water, *J. Chem. Phys.* **79**(2), 926–935. 10.1063/1.445869
56. Salomon-Ferrer, R., Götz, A. W., Poole, D., Le Grand, S., and Walker, R. C. (2013) Routine microsecond molecular dynamics simulations with AMBER on GPUs. 2. explicit solvent particle mesh Ewald, *J. Chem. Theory Comput.* **9**(9), 3878–3888. 10.1021/ct400314y
57. Ryckaert, J.-P., Ciccotti, G., and Berendsen, H. J. (1977) Numerical integration of the cartesian equations of motion of a system with constraints: Molecular dynamics of n-alkanes, *J. Comput. Phys.* **23**(3), 327–341. 10.1016/0021-9991(77)90098-5
58. Miyamoto, S. and Kollman, P. A. (1992) SETTLE: An analytical version of the SHAKE and RATTLE algorithm for rigid water models, *J. Comput. Chem.* **13**(8), 952–962. 10.1002/jcc.540130805
59. Hamelberg, D., Mongan, J., and McCammon, J. A. (2004) Accelerated molecular dynamics: A promising and efficient simulation method for biomolecules, *J. Chem. Phys.* **120**(24), 11919–11929. 10.1063/1.1755656
60. Wereszczynski, J. and McCammon, J. A. (2012) in *Computational Drug Discovery and Design* (Baron, R., ed) pp. 515–524, Springer, New York
61. Beauchamp, K. A., Bowman, G. R., Lane, T. J., Maibaum, L., Haque, I. S., and Pande, V. S. (2011) MSMBuilder2: Modeling conformational dynamics on the picosecond to millisecond scale, *J. Chem. Theory Comput.* **7**(10), 3412–3419. 10.1021/ct200463m
62. McGibbon, R. T. and Pande, V. S. (2015) Variational cross-validation of slow dynamical modes in molecular kinetics, *J. Chem. Phys.* **142**(12), 124105. 10.1063/1.4916292
63. Metzner, P., Noé, F., and Schütte, C. (2009) Estimating the sampling error: Distribution of transition matrices and functions of transition matrices for given trajectory data, *Phys. Rev. E* **80**(2), 021106. 10.1103/PhysRevE.80.021106
64. Phillips, J. C., Braun, R., Wang, W., Gumbart, J., Tajkhorshid, E., Villa, E., Chipot, C., Skeel, R. D., Kale, L., and Schulten, K. (2005) Scalable molecular dynamics with NAMD, *J. Comput. Chem.* **26**(16), 1781–1802. 10.1002/jcc.20289
65. Sievers, F., Wilm, A., Dineen, D., Gibson, T. J., Karplus, K., Li, W., Lopez, R., McWilliam, H., Remmert, M., Söding, J., Thompson, J. D., and Higgins, D. G. (2011) Fast, scalable generation of high-quality protein multiple sequence alignments using Clustal Omega, *Mol. Syst. Biol.* **7**. 10.1038/msb.2011.75
66. Berardini, T. Z., Reiser, L., Li, D., Mezheritsky, Y., Muller, R., Strait, E., and Huala, E. (2015) The *Arabidopsis* information resource: Making and mining the "gold standard" annotated reference plant genome, *Genes.* **53**(8), 474–485. 10.1002/dvg.22877
67. Cock, P. J., Antao, T., Chang, J. T., Chapman, B. A., Cox, C. J., Dalke, A., Friedberg, I., Hamelryck, T., Kauff, F., Wilczynski, B., and de Hoon, M. (2009) Biopython: Freely available Python tools for computational molecular biology and bioinformatics, *Bioinforma.* **25**(11), 1422–

1423. 10.1093/bioinformatics/btp163
68. Rambaut, A. (2014) Figtree 1.4.2, http://tree.bio.ed.ac.uk/software/figtree/

FIGURES

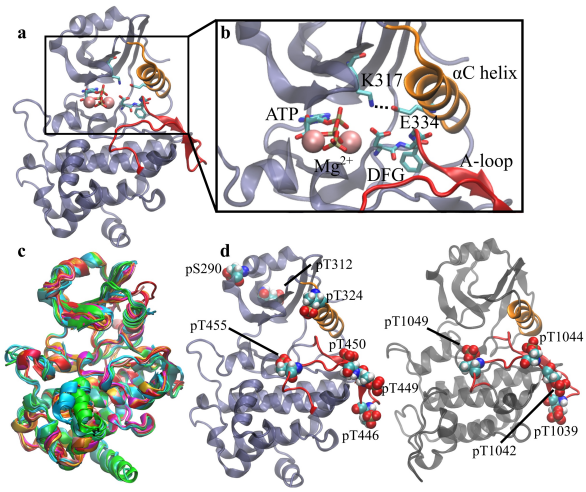

Figure 1: a) The putative BAK1 active state (PDB ID: 3TL8, chain A (51)), with ATP and Mg^{2+} ions taken from previous simulations added. b) Detail of the active site in the BAK1 active-like state. c) Structural alignment of all available crystal structures of the BRI1 (red, pink, and orange) and BAK1 (cyan and green) kinase domains. d) Phosphorylated residues for the simulated BAK1 (left) and BRI1 (right) kinase domains.

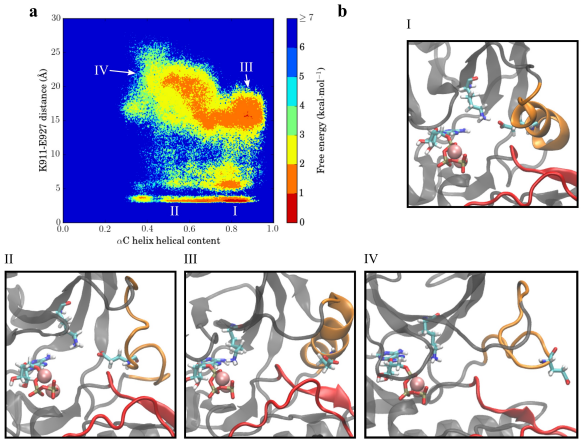

Figure 2: a) Markov state model-weighted free energy landscape of the BRI1 kinase domain. b) (I-IV) BRI1 conformations representing the corresponding regions on the free energy surface in a). I) Active-like structure, II) αC helix disordered structure with an intact K-E salt bridge, III) Src-like inactive structure characterized by a folded αC helix swung distally and a broken K-E salt bridge, IV) structure with a disordered αC helix and a broken K-E salt bridge.

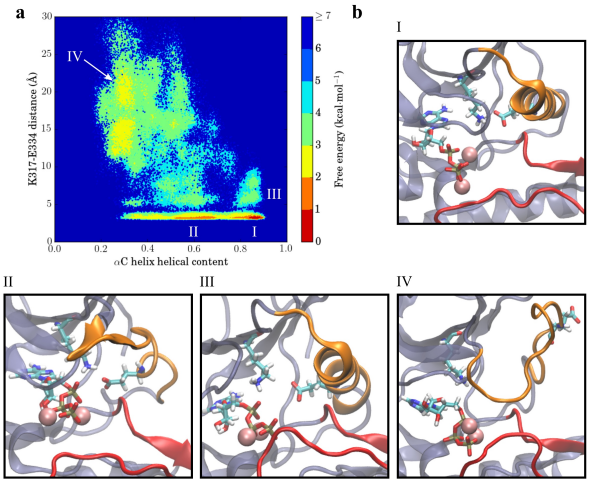

Figure 3: a) Markov state model-weighted free energy landscape of the BAK1 kinase domain. b) (I-IV) BAK1 conformations representing the corresponding regions on the free energy surface in a). I) Active-like structure, II) αC helix disordered structure with an intact K-E salt bridge, III) structure with a folded and properly positioned (as in the active-like state) αC helix but with a broken K-E salt bridge, IV) structure with a disordered αC helix and a broken K-E salt bridge.

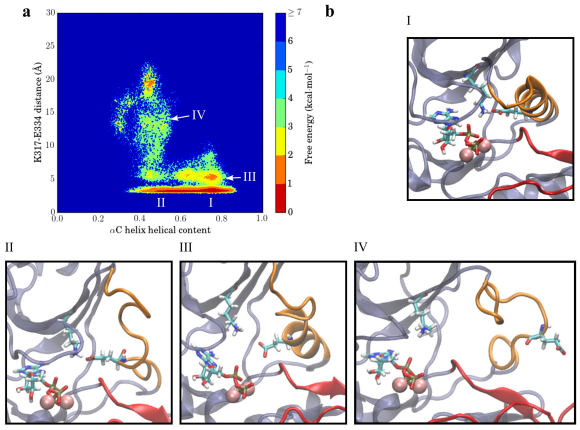

Figure 4: a) Markov state model-weighted free energy landscape of the BAK1-Src kinase domain. b) (I-IV) BAK1-Src conformations representing the corresponding regions on the free energy surface in a). I) Active-like structure, II) αC helix disordered structure with an intact K-E salt bridge, III) structure with a folded and properly positioned (as in the active-like state) αC helix but with a broken K-E salt bridge, IV) structure with a disordered αC helix and a broken K-E salt bridge.

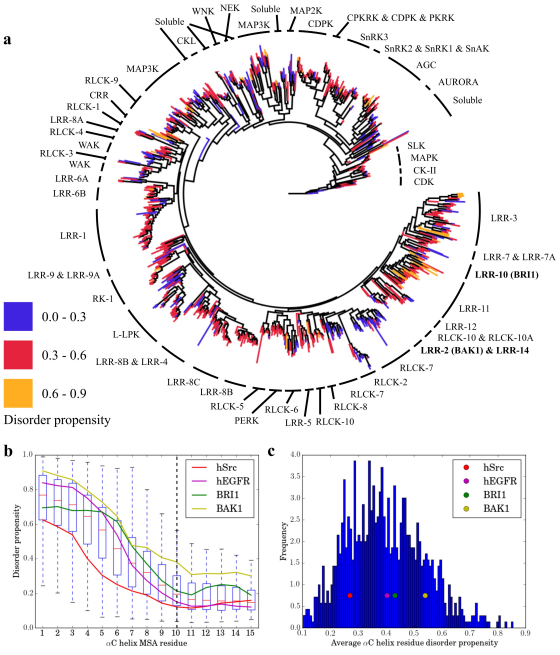

Figure 5: a) The average disorder propensity of the 15 MSA residues corresponding the BAK1 αC helix mapped onto a maximum likelihood phylogenetic tree of the *A. thaliana* kinome (25). b) Profile of the predicted disorder across the 15 MSA residues corresponding the BAK1 αC helix for hSrc, hEGFR, BRI1, and BAK1. Also included is a box plot showing the means and quartiles of predicted disorder propensity distributions for each residue across the 930 included sequences of the *A. thaliana* kinome. The conserved E334 (BAK1 numbering) is denoted by the vertical dashed line. c) Histogram of the average αC helix predicted disorder propensities calculated for a).

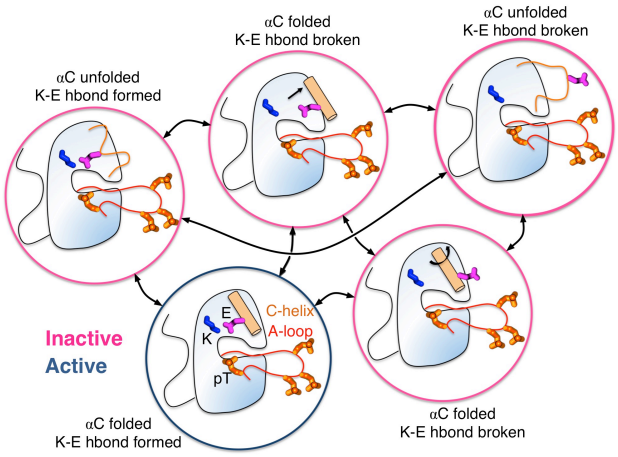

Figure 6: The conformational states obtained from molecular simulations reveal different mechanisms of catalytic domain inhibition due to the conformational change in the αC helix.

Molecular dynamics simulations reveal the conformational dynamics of Arabidopsis thaliana BRI1 and BAK1 receptor-like kinases

Alexander S Moffett, Kyle W Bender, Steven C Huber and Diwakar Shukla

J. Biol. Chem. published online May 30, 2017